Photonic Sensors (2012) Vol. 2, No. 3: 259–270

DOI: 10.1007/s13320-012-0067-2 **Photonic Sensors**

Regular

Sensitivity and Performance of Cavity Optomechanical Field Sensors

Stefan FORSTNER, Joachim KNITTEL, Eoin SHERIDAN, Jon D. SWAIM, Halina RUBINSZTEIN-DUNLOP, and Warwick P. BOWEN*

School of Mathematics and Physics, University of Queensland, St Lucia, Queensland 4072, Australia

*Corresponding Author: Warwick P. BOWEN E-mail: w.bowen@uq.edu.au

Abstract: This article describes in detail a technique for modeling cavity optomechanical field sensors. A magnetic or electric field induces a spatially varying stress across the sensor, which then induces a force on mechanical eigenmodes of the system. The force on each oscillator can then be determined from an overlap integral between magnetostrictive stress and the corresponding eigenmode, with the optomechanical coupling strength determining the ultimate resolution with which this force can be detected. Furthermore, an optomechanical magnetic field sensor is compared to other magnetic field sensors in terms of sensitivity and potential for miniaturization. It is shown that an optomechanical sensor can potentially outperform state-of-the-art magnetometers of similar size, in particular other sensors based on a magnetostrictive mechanism.

Keywords: Cavity optomechanics, magnetic field sensors, magnetostriction, integrated microcavity

1. Introduction

Ultra-sensitive field sensors, particularly magnetometers, play important roles in multiple fields including geology, mineral exploration, archaeology, material-testing, and medicine [1]. Thus, many different types of magnetometer have been developed taking advantage of a range of different physical phenomena [1, 2] including giant magnetoresistance in thin films [3], magnetostriction [4], magnetic force microscopy [5], quantum interference in superconductors [6], the Hall effect [7], optical pumping [8], electron spin resonances in solids [9], and even Bose-Einstein condensation [10]. Currently, the most practical and widely used ultra-low field magnetometer is based on the superconducting quantum interference device (SQUID) [11], which achieve a sensitivity of up to $1\,\mathrm{fT\,Hz^{-1/2}}$ [1], enabling SQUIDs to detect single flux quanta. Their sensitivity is only outperformed by spin exchange relaxation-free (SERF) magnetometers, which achieve a record sensitivity of $160\,\mathrm{aT\,Hz^{-1/2}}$ at room temperature [8].

A sensor of small geometric dimensions, combined with high sensitivity, is a requirement for many applications. For example in low field nuclear magnetic resonance imaging [12, 13], the sensitivity of the instruments can be enhanced by reducing the distance between the sample and the magnetic field sensor. This also applies to investigations in the field of solid state physics and superconductivity [14, 15]. It is even more relevant for measurements of single dipole moments, as the magnetic dipole-field decays with the distance r as $1/r^3$. In medical applications, richer diagnostic information is obtained by imaging the magnetic field distribution with the highest

Received: 8 June 2012 / Revised version: 16 June 2012

possible resolution and sensitivity. For example, magneto-cardiography (MCG) [1, 16], imaging of the magnetic fields generated by the human heart, relies on signals in the low pT-range. Neurons in the human brain generate even weaker fields, with flux densities between 10 fT (for the celebral cortex [17]) and 1 pT (for synchronous and coherent activity of the thalamic pacemaker cells, resulting in α-rhythm [18]). Highly sensitive magnetometers with high spatial and temporal resolution are necessary to image such fields [17]. Thus, a dense 2-dimensional array of sensors with simple readout and uncomplicated handling is the ideal platform to measure magnetic field distributions with good spatial resolution.

Cavity optomechanical systems have recently been demonstrated as the basis for a new form of field sensor [19], where the cavity optical resonance frequencies are coupled to the mechanical deformation of the cavity structure as depicted in Fig. 1. The cavity optomechanical system is functionalized by the attachment of a material which responds mechanically to an applied field, which could be, for example, an electric or a magnetic field. The response of the material to the applied field stresses the mechanical structure of the cavity. This causes a shift in optical resonance frequencies of the cavity which can be read out using an optical field giving a measurement of the applied field. By engineering both high quality mechanical vibrations in the mechanical structure and high optical quality resonances in the optical cavity, the sensitivity of the measurement is doubly enhanced. The magnetometer demonstrated in [19] was based on lithographically fabricated optical microtoroidal resonators coupled to the magnetostrictive material Terfenol-D. High quality optical and mechanical resonances are present in microtoroids, and Terfenol-D stretches significantly at room temperature under applied magnetic fields resulting in experimental sensitivities in the range of one hundred $nT \cdot Hz^{-1/2}$. Theoretical sensitivities in the $pT\,Hz^{-1/2}$ range predicted for an optimized geometry of this construction [19, 20]. Furthermore, a combination of lithographic fabrication and fiber or waveguide coupling, makes these devices amenable to expansion into arrays.

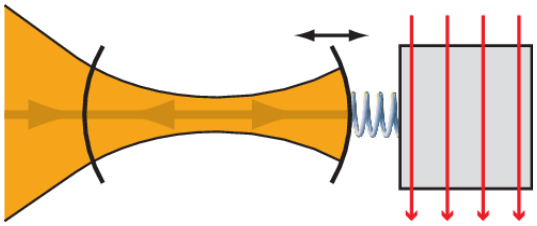

Fig. 1 A cavity optomechanical field sensor, illustrated via the example of a Fabry-Perot-type cavity with a harmonic spring attached to one of the mirrors.

Here, we elaborate in detail on the eigenmode based method for the calculation of the predicted sensitivity of general cavity optomechanical field sensors presented in [21]. Furthermore, we compare the performance achievable by cavity optomechanical magnetometers presented in [19, 20] to other types of magnetometers.

2. Concept of a cavity optomechanical field sensor

The field of cavity optomechanics results from the coalescence of two previously separate areas of research, optical microcavities and mechanical microresonators. An optomechanical system is most generally characterized by its ability to couple optical and mechanical degrees of freedom.

Light acts on mechanical degrees of freedom via radiation pressure. This aspect of optomechanics has been subject to intense research in the past decades and has first been experimentally described in large-scale interferometric gravitational wave experiments [22]. In 1967, Braginsky *et al.* recognized that radiation pressure gives rise to the effect of dynamical backaction [23], laying the foundation for the description of parametric amplification and backaction-cooling [24, 25]. A main goal of the field of optomechanics is to observe quantum phenomena in mechanical systems. Cooling into the quantum ground state has very

recently been achieved, both in nano-electromechanical systems (NEMS) [26] and cavity optomechanical systems (COMS) [27].

Reciprocally, mechanical displacements x act on optical degrees of freedom, as they modify the optical path length and manifest as a measurable change in the cavities resonance frequency Ω.. This relationship is quantified by the optomechanical coupling constant

$$g = \frac{d\Omega}{dx}. \tag{1}$$

There are methods to lock the light field to the full width at half maximum (FWHM) or maximum of an optical resonance. Then, the intensity or phase signal of the transmitted light can be measured, respectively. In both cases, the measured photocurrent I, which is proportional to the resonance frequency shift $\delta\Omega$ and thus to the displacement x, is enhanced by the optical quality factor Q_{opt} relative to the measurement noise

$$I \propto \delta\Omega \cdot Q_{opt} \propto x \cdot Q_{opt}. \tag{2}$$

This makes high quality optical microcavities ultra-sensitive position sensors. On the microscale, toroidal whispering gallery mode resonators reach shot-noise limited displacement sensitivities of down to 10^{-19} m Hz$^{-1/2}$ [28]. The measurement of random thermal motion at room temperature is now achieved by a variety of optomechanical systems [25].

By employing a medium capable of transducing electric or magnetic field energy into elastic energy, an external field exerts a force on one or several mechanical degrees of freedom of the COMS, which is then transduced into a displacement.

As force-sensors, COMS are outperformed by NEMS, i.e. NEMS cantilevers [29]. Their extremely low mass makes them receptive to minute force and mass variations enabling even single molecule mass spectroscopy. COMS have a larger mass and thus seem to be less suited for these applications. However, in field sensing the larger volume of COMS increases the coupling to external fields and makes COMS potentially competitive for ultra-low field sensing applications.

Toroidal whispering-gallery-mode (WGM) resonators are prominent representatives of COMS and combine simultaneously high quality optical resonators ($Q_{opt} \approx 10^8$) and mechanical resonators ($Q_{mech} \approx 10^4$, $m_{eff} \sim \geqslant 10$ng). Other actively researched COMS include photonic crystal cavities [27, 30], nanomembranes made from GaAs [31] or SiN [32], ZnO-microwires [33], and many others [34–37].

3. Force and field sensitivity of a general optomechanical sensor

3.1 Eigenmodes

The mechanical motion of the COMS can be decomposed into its intrinsic vibrational eigenmodes, allowing the system to be described as a set of damped harmonic oscillators. In an isotropic homogeneous medium, the equation of motion for the mechanical vibration is given by the elastic wave equation [38]:

$$\rho\ddot{\vec{u}}(\vec{r},t) = (\lambda+\mu)\vec{\nabla}\cdot\left(\vec{\nabla}\cdot\vec{u}(\vec{r},t)\right) + \mu\vec{\nabla}^2\vec{u}(\vec{r},t) \tag{3}$$

where the vector field $\vec{u}(\vec{r},t)$ denotes the displacement of an infinitesimally small cubic volume element at the initial position $\vec{r}$ and time t, ρ is the density of the material, and λ and μ are the Lamé constants:

$$\lambda = \frac{\sigma E}{(1+\sigma)(1-2\sigma)} \tag{4}$$

$$\mu = \frac{E}{2(1+\sigma)} \tag{5}$$

with σ and E being Poisson's ratio and Young's modulus, respectively. Using the ansatz $\vec{u}(\vec{r},t) = \vec{\psi}(\vec{r})X(t)$ leads to a complete set of orthonormal eigenmode solutions:

$$\vec{u}_q(\vec{r},t) = X_q(t)\vec{\psi}_q(\vec{r}) \tag{6}$$

where $X_q(t)$ is the time dependent oscillation of eigenmode q, and $\vec{\psi}_q(\vec{r})$ is its position dependent mode shape function. $\vec{\psi}_q(\vec{r})$ can be normalized

such that $\int_V \vec{\psi}_p(\vec{r})\cdot\vec{\psi}_q(\vec{r})d^3r = V\delta_{pq}$, with V being the spatial volume of the oscillator. When inserted into (3), this yields the new equation of motion

$$\ddot{X}_q(t) = \left[\frac{(\lambda+\mu)\vec{\nabla}\cdot\left(\vec{\nabla}\cdot\vec{\psi}_q(\vec{r})\right)+\mu\vec{\nabla}^2\vec{\psi}_q(\vec{r})}{\rho\vec{\psi}_q(\vec{r})}\right]X_q(t). \quad (7)$$

Since the left hand side of this equation is evidently independent of the position $\vec{r}$, so must be the right hand side, with the term in square brackets being constant and causing the elastic restoring force of the material. For the mechanical motion to be stable, this term must also be negative, and with the benefit of hindsight, we define it to equal $-\omega_q^2$ here. The equation of motion is then separable into one spatial and one temporal equation of motion

$$(\lambda+\mu)\vec{\nabla}\cdot\left(\vec{\nabla}\cdot\vec{\psi}_q(\vec{r})\right)+\mu\vec{\nabla}^2\vec{\psi}_q(\vec{r}) = -\rho\omega_q^2\vec{\psi}_q(\vec{r}) \quad (8)$$

$$\ddot{X}_q(t) = -\omega_q^2 X_q(t) \quad (9)$$

with

$$\omega_q^2 = -\frac{(\lambda+\mu)\vec{\nabla}\cdot\left(\vec{\nabla}\cdot\vec{\psi}_q(\vec{r})\right)+\mu\vec{\nabla}^2\vec{\psi}_q(\vec{r})}{\rho\vec{\psi}_q(\vec{r})}. \quad (10)$$

The second equation here is, of course, just Hooke's law for an oscillator with resonance frequency ω_q and spring constant $k_q = M\omega_q^2$, where M is the mass of the oscillator. Hence, as expected, the elastic nature of the material causes the amplitude of each eigenmode to independently oscillate at a characteristic frequency just like a mass on a spring. Solving the first equation for the spatial eigenmodes of vibration is generally difficult, and in many cases only numerical solutions are possible, however the solution yields a complete set of orthogonal eigenmodes each with a characteristic value for ω_q. The total displacement vector field $\vec{u}_q(\vec{r},t)$ for a general motion of the oscillator can of course be expanded as

$$\vec{u}(\vec{r},t) = \sum_q \vec{u}_q(\vec{r},t) = \sum_q X_q(t)\vec{\psi}_q(\vec{r}) = \sum_q \vec{\psi}_q(\vec{r})X_q(t=0)e^{i\omega_q t}. \quad (11)$$

3.2 Including external forces and dissipation

Let us now consider the response of the mechanical modes to a force density $\vec{f}(\vec{r},t)$ applied to the mechanical structure. Including this force density, the elastic wave (3) becomes

$$\rho\ddot{\vec{u}}(\vec{r},t) = (\lambda+\mu)\vec{\nabla}\cdot\left(\vec{\nabla}\cdot\vec{u}(\vec{r},t)\right)+\mu\vec{\nabla}^2\vec{u}(\vec{r},t)+\vec{f}(\vec{r},t). \quad (12)$$

Expanding the displacement vector field $\vec{u}(\vec{r},t)$ as in (11) and inserting the definition of ω_q [see (10)] yields

$$\rho\sum_q \ddot{X}_q(t)\cdot\vec{\psi}_q(\vec{r})_{pq} = -\rho\sum_q X_q(t)\vec{\psi}_q(\vec{r})\omega_q^2 + \vec{f}(\vec{r},t). \quad (13)$$

After multiplying both sides with $\vec{\psi}_p(\vec{r})$ and integrating over the spatial volume V of the oscillator, the orthonormality relation $\int_V \overrightarrow{\psi_p}(\vec{r})\bullet\vec{\psi}_q(\vec{r})d^3r = V\delta_{pq}$ can be exploited, leading to

$$\rho\sum_q \ddot{X}_q(t)V\delta_{pq} = -\rho\sum_q X_q(t)\omega_q^2\delta_{pq} + \int_V \vec{\psi}_q(\vec{r})\cdot\vec{f}(\vec{r},t)d^3r \quad (14)$$

$$\Leftrightarrow M\left(\ddot{X}_p(t)+\omega_p^2 X_p(t)\right) = \int_V \vec{\psi}_q(\vec{r})\cdot\vec{f}(\vec{r},t)d^3r \quad (15)$$

where we introduce the total mass of the oscillator $M = \rho V$. In order to obtain an expression for the right hand side of (15), we separate the force density into temporally and spatially varying components, which it is convenient to express in terms of the mechanical eigenmodes of the system

$$\vec{f}(\vec{r},t) = \frac{1}{V}\sum_q F_q(t)\vec{\psi}_q(\vec{r}). \quad (16)$$

The right hand side of (15) then computes to

$$\int_V \vec{\psi}_q(\vec{r})\cdot\vec{f}(\vec{r},t)d^3r = \frac{1}{V}\sum_q F_q(t)V\delta_{pq} = F_p(t), \quad (17)$$

and $F_q(t)$ is identified as the force in Newtons acting on the mechanical eigenmode q. This yields independent equations of motion for each mechanical mode

$$M\left[\ddot{X}_q(t)+\Gamma_q\dot{X}_q(t)+\omega_q^2 X_q(t)\right] = F_q(t) \quad (18)$$

where we have introduced independent linear decay with rate Γ_q to each of the mechanical eigenmodes as

is typical of damping in mechanical oscillators. The force $F_q(t)$ can contain forces from a range of different sources. The three forces relevant are the random thermal force $F_{th,q}(t)$, the radiation pressure force from the presence of the optical field used to monitor the mechanical motion $F_{rp,q}(t)$, and the force applied by the signal field which we aim to detect $F_{\mathrm{sig},q}(t)$; with the total force $F_q(t) = F_{th,q}(t) + F_{rp,q}(t) + F_{sig,q}(t)$. The thermal force can be shown from the fluctuation-dissipation theorem to equal [39]

$$F_{th,q}(t) = \sqrt{2M\Gamma_q k_B T}\,\xi_q(t) \tag{19}$$

where $k_B = 1.381$ m^2 kg s^{-1} K^{-1} is the Boltzmann constant, T is the temperature of the system, and $\varepsilon_q(t)$ is a unit white noise Wiener process. The radiation pressure force can be determined from Hamiltonian mechanics using the optomechanical interaction Hamiltonian [40]

$$H_{I,q} = \hbar G_q X_q(t) n(t) \tag{20}$$

where $G_q = d\Omega_q / d\mathrm{X}_q$ is the optomechanical coupling strength, and $q(t)$ is the number of photons within the optical resonator. The result is

$$F_{rp,q}(t) = \frac{\partial H_{I,q}}{\partial X_q} = \hbar G_q n(t). \tag{21}$$

Hence, the equation of motion for the mechanical mode q can be expressed as

$$\begin{aligned} &M\left[\ddot{X}_q(t) + \Gamma_q \dot{X}_q(t) + \omega_q^2 X_q(t)\right] \\ &= \sqrt{2M\Gamma_q k_B T}\,\xi_q(t) + \hbar G_q n(t) + F_{sig,q}(t). \end{aligned} \tag{22}$$

3.3 Conversion to measurable parameters

In the case considered here of optical measurement, the measured signal is the frequency shift on the optical mode $\delta\Omega_q = \Omega_0 - \Omega_q$ where Ω_0 is the unperturbed optical resonance frequency of an intrinsic optical mode of the cavity, and Ω_q is the modified resonance frequency as a result of the mode displacement $X_q(t)$. Of course, the total frequency shift due to the action of several mechanical eigenmodes is given by $\delta\Omega = \sum_q \delta\Omega_q$. Equation (22) completely describes the motion of the qth mechanical eigenmode of the oscillator. In principle, the resulting frequency shift on the optical mode can be determined from the optomechanical coupling rate $G_q = d\Omega_q / dX_q$ to

$$\delta\Omega_q = G_q X_q(t). \tag{23}$$

However, in general neither the displacement parameter $X_q(t)$ nor the raw optomechanical coupling rate G_q are directly accessible in experiments. The measured frequency shift on the optical mode, which provides the change in optical path length $x(t)$ rather than $X_q(t)$. Hence, to apply (18) to optical measurements made on a cavity optomechanical system, the length coordinate must be rescaled in terms of this measured variable. Furthermore, since the optomechanical coupling rate is defined in terms of the optical resonance frequency shift for a given displacement of the mechanical oscillator, the use of a different length scale results in a modification to this rate. The raw optomechanical coupling rate G_q must therefore also be replaced with the measurable optomechanical coupling rate g. It is defined with respect to the optical path length x, and therefore, it does not depend on the displacement pattern of the particular mechanical eigenmode q but only on the geometry of the oscillator. The purpose of this section is to mathematically perform the transformation to these measurable parameters. To rescale the position coordinate, we recognize that the optomechanical interaction energy must remain constant under a change in the coordinate system, so that

$$H_{I,q} = \hbar G_q X_q(t) n(t) = \hbar g x_q(t) n(t) \tag{24}$$

where x_q is the change in the optical path length as a result of motion of the qth mechanical mode, and of course the total change in the optical path length is just the sum over x_q, $x = \sum_q x_q$. The directly measurable optomechanical coupling strength in the new optically defined coordinate system is $g = d\Omega_q / dx_q$. Consequently, we have

$$X_q(t) = \frac{g}{G_q} x_q(t). \tag{25}$$

Similarly, since the potential energy of the

mechanical mode U_q must be constant under the co-ordinate transformation, we have

$$U_q = \frac{1}{2} M \omega_q^2 X_q^2(t) = \frac{1}{2} m_q \omega_q^2 x_q^2(t), \quad (26)$$

so that

$$\frac{M}{m_q} = \left(\frac{x_q}{X_q} \right)^2 = \left(\frac{G_q}{g} \right)^2. \quad (27)$$

Rearranging (27), we find

$$G_q = g \sqrt{\frac{M}{m_q}}. \quad (28)$$

For the purpose of theoretical modeling of an optomechanical system, the ratio g/G_q can be calculated using a weighting function $\vec{\omega}(\vec{r})$, which quantifies the frequency shift created by a displacement $\vec{\Psi}_q(\vec{r})$ of the volume element at position $(\vec{r})$ (compare [40])

$$\frac{g}{G_q} = \int_V \vec{w}(\vec{r}) \cdot \vec{\psi}(\vec{r}) d^3 r = \sqrt{\frac{M}{m_q}}. \quad (29)$$

The exact determination of $\vec{\omega}(\vec{r})$ can be complicated, however, useful approximations can be made, dependent on the structure of a particular optomechanical system. For example in a Fabry-Perot cavity, the effect of a mirror displacement at a position $\vec{r}$ normal to its surface is weighted by the normalized electromagnetic flux density at that location [41]. In whispering-gallery-mode cavities, one can approximate $\vec{\omega}(\vec{r})$ by considering the effect of a mechanical displacement of the cavity boundary on the electromagnetic energy stored in the optical mode [40]. However, in experiments it is generally easier to directly determine $\sqrt{M/m_q}$, and thus g/G_q [from (27)] by measurement, which in these cases, makes the rather complicated weighting function redundant. By substituting for $X_q(t)$ and G_q in (22), and re-scaling with $\sqrt{M/m_q}$, an equation of motion for the mechanical oscillator eigenmodes in terms of measurable parameters is finally obtained

$$\begin{aligned} & m\left[\ddot{x}_q(t) + \Gamma_q \dot{x}_q(t) + \omega_q^2 x_q(t) \right] \\ & = \sqrt{2 m_q \Gamma_q k_B T} \xi_q(t) + \hbar g n(t) + \sqrt{\frac{m_q}{M}} F_{sig,q}(t). \end{aligned} \quad (30)$$

The first term on the right hand side can be interpreted as an effective thermal force, related to measurable quantities [42]. This equation of motion is identical in form to the unscaled equation of motion, except for a scaling of the signal force by the ratio of optomechanical coupling rates.

3.4 Force and field sensitivity

To determine the sensitivity of the cavity optomechanical sensor, we start by solving (30) in the frequency domain. Taking the Fourier transform, we find

$$\begin{aligned} & x_q(\omega) = \\ & \chi_q(\omega) \left[\sqrt{2 m_q \Gamma_q k_B T} \xi_q(\omega) + \hbar g n(\omega) + \sqrt{\frac{m_q}{M}} F_{sig,q}(\omega) \right] \end{aligned} \quad (31)$$

where $x_q = [m_q(\omega_q^2 - \omega^2 - i\Gamma_q \omega)]^{-1}$ is the susceptibility of the qth mechanical mode. As mentioned before, this causes an observable shift in the resonance frequency of the optical resonator. The magnitude can be determined from (23) and (25) as $\delta\Omega_q = g x_q(t)$ so that in the frequency domain we have

$$\delta\Omega_q(\omega) = g \chi_q(\omega) \left[\sqrt{2 m_q \Gamma_q k_B T} \xi_q(\omega) + \hbar g n(\omega) + \sqrt{\frac{m_q}{M}} F_{sig,q}(\omega) \right]. \quad (32)$$

The spectral power contributions from the signal $S_{\Omega\Omega}^{sig}(\omega)$ and noise $S_{\Omega\Omega}^{noise}(\omega)$ in the final detected signal can then be calculated as

$$S_{\Omega\Omega}^{sig,q} = \left| \left\langle \delta\Omega_q(\omega) \right\rangle \right|^2 \quad (33)$$

$$S_{\Omega\Omega}^{noise,q} = \left\langle \left| \delta\Omega_q(\omega) \right|^2 \right\rangle - \left| \left\langle \delta\Omega_q(\omega) \right\rangle \right|^2 + S_{\Omega\Omega}^{meas}(\omega) \quad (34)$$

where we have included the measurement noise term $S_{\Omega\Omega}^{meas}(\omega)$ which accounts for shot and frequency noise on the laser field and other noise sources such

as electronic noise in the detectors used to measure the optical field. As this type of noise is not caused by a shift in the optical coordinate x, the measurement noise is independent of the mechanical mode q. Taking a signal force at the single frequency $\omega_{sig}, F_{sig,q}(\omega) = F_{sig,q}\delta(\omega - \omega_{sig})$, we find the spectral contribution of the signal

$$S_{\Omega\Omega}^{sig,q}(\omega) = g^2 \left|\chi_q(\omega)\right|^2 \frac{m_q}{M} F_{sig,q}^2 \delta(\omega - \omega_{sig}) \qquad (35)$$

where we have used the fact that $\langle \xi_q(\omega) \rangle = 0$ and $\langle n(\omega) \rangle = 0$ for $\omega \neq 0$. To calculate the noise contribution from the fact that $\xi_q(t)$ is unit white noise such that $\langle |\xi(t)|^2 \rangle = 1$, using Parseval's theorem we obtain $\langle |\xi(\omega)|^2 \rangle = 1$, and we define the fluctuations in the photon number within the optical resonator $\delta n(\omega) = n(\omega) - \langle n(\omega) \rangle = n(\omega)$. This yields

$$S_{\Omega\Omega}^{noise,q}(\omega) = g^2 \left|\chi_q(\omega)\right|^2 \left[2m_q \Gamma_q k_B T + \hbar g^2 \left\langle \delta n_{qn}(\omega)^2 \right\rangle \right] + S_{meas}(\omega). \qquad (36)$$

The minimum detectable force $F_{sig,q}^{min}$ is obtained by integrating signal and noise contributions over the bandwidth of the measuring system resolution bandwidth (RBW) and setting the signal and noise powers equal such that the signal-to-noise ratio is unity:

$$\frac{F_{sig}^{min}}{\sqrt{RBW}} = \frac{1}{c_{act}} \sqrt{2M\Gamma_q k_B T + \frac{M}{m_q} \left[\hbar g^2 \left\langle \delta n_{qn}(\omega)^2 \right\rangle + \frac{S_{meas}}{g^2 \left|\chi_q(\omega)\right|^2} \right]}. \qquad (37)$$

In order to determine the sensitivity to an applied spatially uniform field $\vec{\Phi}(t) = \vec{\Phi} e^{i\omega_{sig} t}$, the body force density $\vec{f}_{sig}(\vec{r},t)$ due to the applied field must be determined. It can be extracted from a finite element model or estimated analytically. The force on a specific mechanical eigenmode can then be found via

$$F_{sig,q}(t) = \int_V \vec{\psi}_q(\vec{r}) \cdot \vec{f}_{sig}(\vec{r},t) d^3 r, \qquad (38)$$

which follows from (17) and (18) and the orthonormality relation for mechanical eigenmodes. In typical circumstances, a linear relationship will exist between this force and the amplitude of the applied field, such that $F_{sig,n} = c_{act} |\vec{\Phi}|$ where the actuation constant c_{act} determines the strength of the coupling. c_{act} depends on the material properties of the transduction medium, and it is determined for the case of a magnetostrictive material in [20]. The minimum detectable field is then simply found by substituting this relationship into (37):

$$\left|\vec{\Phi}\right|^{min} \cdot \sqrt{t_{meas}} = \frac{\left|\vec{\Phi}\right|^{min}}{\sqrt{RBW}} = \frac{1}{c_{act}} \sqrt{2M\Gamma_q k_B T + \frac{M}{m_q} \left[\hbar g^2 \left\langle \delta n_{qn}(\omega)^2 \right\rangle + \frac{S_{meas}}{g^2 \left|\chi_q(\omega)\right|^2} \right]} \qquad (39)$$

where $t_{meas} = 1/RBW$ is the minimum time required to detect a field of amplitude $|\vec{\Phi}|^{min}$ with a signal-to-noise ratio of one. It can be seen that, in the usual limit where the radiation pressure force due to photon number fluctuations is negligible, high mechanical quality factor $Q_q = \omega_q / \Gamma_q$ is always advantageous for precise sensing, reducing the thermal noise, and also, on resonance, the effect of the measurement noise through its contribution to $x_q(\omega) = [m_q(\omega_q^2 - \omega^2 - i\Gamma_q \omega)]^{-1}$.

In this limit, a low effective mass is beneficial for sensing, as its total effect will be a suppression of the measurement noise. Also improving the optical quality factor of the cavity is of advantage, as common measurement techniques convert a frequency shift signal to an amplitude- or phase-signal, which is enhanced as Q_{opt} relative to the measurement noise [see (2)].

3.5 Quantum limited detection

In the following, the fundamental quantum limit for the detection of a field by the means of a cavity optomechanical system is analyzed. For the case of an ideal quantum limited measurement, the corresponding noise $S_{\Omega\Omega}^{meas}$ is constituted by the fundamental imprecision of the measurement $S_{\Omega\Omega}^{im,qn}$

due to the limited photon number (shot noise) [40]

$$S_{\Omega\Omega}^{meas}(\omega)=S_{\Omega\Omega}^{im,qn}(\omega)=\frac{\omega^2-(\kappa/2)^2}{4\bar{n}^2\kappa}, \quad (40)$$

where κ is the decay rate of the optical mode, and $\bar{n}$ is the mean photon number in the system. The quantum limited fluctuation of the radiation pressure force is known as quantum back-action [40]

$$\begin{aligned} S_{\Omega\Omega}^{ba,qn}(\omega)&=\hbar g^2\left\langle \delta n_{qn}(\omega)^2\right\rangle \\ &=\left|\chi_q(\omega)\right|\frac{\hbar\bar{n}^2g^4\kappa}{\omega^2-(\kappa/2)^2} \end{aligned} \quad (41)$$

where $\delta n_{qn}(\omega)$ denotes the quantum limited photon number fluctuation. Both $S_{\Omega\Omega}^{im,qn}$ and $S_{\Omega\Omega}^{ba,qn}$ can be derived from the quantum Langevin equations [43]. From the above equations, it is immediately clear that $S_{\Omega\Omega}^{im,qn}\propto 1/\bar{n}^2$, whereas $S_{\Omega\Omega}^{ba,qn}\propto\bar{n}^2$ and thus an optimal mean photon number $\bar{n}_{opt}$ can be found by minimizing the sum $S_{\Omega\Omega}^{qn}=S_{\Omega\Omega}^{im,qn}+S_{\Omega\Omega}^{ba,qn}$

$$\bar{n}_{opt}=\frac{m_q\Gamma_q\omega_q}{2g^2\hbar\kappa}\left(\omega_q^2+(\kappa/2)\right). \quad (42)$$

Inserting this into (40) and (41) yields the simple result

$$S_{\Omega\Omega}^{im,SQL}(\omega)=\hbar g^2\left|\chi_q(\omega)\right|, \quad (43)$$

which is known as the standard quantum limit. It corresponds to a measurement wherein the fundamental Heisenberg-uncertainty is equally distributed between position and momentum quadrature. This can be seen from the fundamental inequality in the imprecision-back action product [44]

$$S_{\Omega\Omega}^{im}\cdot S_{\Omega\Omega}^{ba}\geqslant\frac{\hbar}{2}, \quad (44)$$

with the mechanical displacement spectrum $S_{xx}^{im}=S_{\Omega\Omega}^{im}/g_q^2$ and the force spectrum $S_{FF}^{ba}=S_{\Omega\Omega}^{ba,qn}/g_q^2|x_q|$. Identical position and momentum uncertainties at the Heisenberg-limit correspond to

$$S_{\Omega\Omega}^{im,SQL}(\omega)=\left|\chi_q\right|^2S_{FF}^{ba,SQL}=\left|\chi_q\right|\frac{\hbar}{2}, \quad (45)$$

and we retrieve the standard quantum limit by adding its contributions

$$S_{\Omega\Omega}^{SQL}(\omega)=g^2S_{xx}^{im,SQL}+g^2\left|\chi_q\right|^2S_{FF}^{ba,SQL}. \quad (46)$$

Consequently, the quantum limit for field detection follows by inserting $S_{xx}^{SQL}(\omega)$ into (39).

$$\begin{aligned} \left|\vec{\Phi}\right|^{min,SQL}\cdot\sqrt{t_{meas}}&=\frac{\left|\vec{\Phi}\right|^{min,SQL}}{\sqrt{RBW}} \\ &=\frac{1}{c_{act}}\sqrt{2M\Gamma_qk_BT+\frac{\hbar M}{\left|\chi_q(\omega)\right|m_q}}. \end{aligned} \quad (47)$$

As discussed regarding (39), a high mechanical quality factor (i.e. a low damping Γ_q) and a low effective mass are favorable for sensing. The optical quality factor does not have a direct influence on the quantum limited detection sensitivity, however it can still be considered an advantage as a lower optical loss rate decreases the mean photon number $\bar{n}_{opt}$ required to achieve measurements at the quantum limit, making them technically more feasible.

4. Comparison of a cavity optomechanical magnetometer with other state-of-the-art magnetometers

Cavity optomechanical field sensors are particularly attractive as miniature magnetometers, with sensitivities in the range of $\mathrm{nT\,Hz^{-1/2}}$ already demonstrated in a recent experiment and a theoretical model predicting sensitivities below one $\mathrm{pT\cdot Hz^{-1/2}}$ [19, 20]. It is interesting to compare the results presented in [19, 20] to several types of state-of-the-art magnetic field sensors such as SQUIDs, SERFs, Hall sensors and in particular other magnetometers based on a magnetostrictive mechanism. In Fig. 2, the detection volume of several recently developed magnetometers is shown versus their sensitivities. This measure is particularly useful for evaluation of the ability of different magnetometers to detect the field from a magnetic dipole, as dipole fields decay with r^{-3} as a function of the distance r from their source, and for magnetic field imaging where a high spatial density of sensors is required. Generally, the volume is representative of the typical distance of a sample to

the center of the sensor. However, technical constraints cause this distance to be much greater in some sensors, such as SQUIDs which require cryogenic cooling.

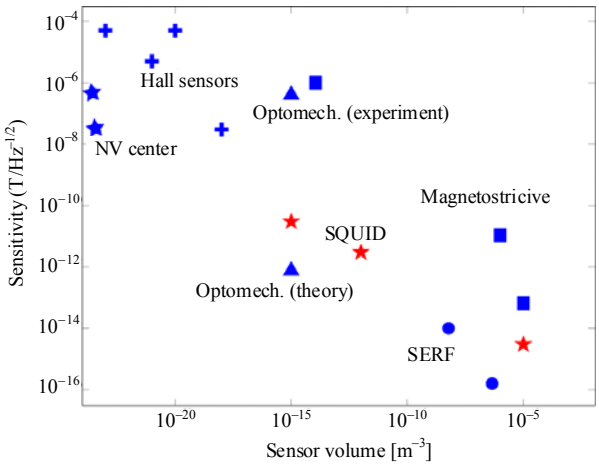

Fig. 2 Sensitivity vs. detection volume of some modern state-of-the-art magnetic field sensors. Shown are SERF magnetometers (circles) [8, 45], SQUIDs (small asterisk) [46–48], Hall-sensors (crosses) [49, 50], nitrogen-vacancy(NV)-center based magnetometers (bold asterisk) [51, 52]. Magnetostrictive sensors (rectangles) can be found in various sizes and their sensitivity generally lies above modern sensors of comparable size [4, 53, 54], and their sensitivity can be greatly enhanced by coupling the magnetostrictive material to an optomechanical cavity (triangles), as described in this article (the figure partly based on [51]).

Hall sensors use the Lorentz-force on charge carriers in a semiconductor to detect magnetic fields and are today among the most commonly used magnetic field sensors due to their cost efficiency and flexibility. They have recently been fabricated on the sub-micron scale [49, 50]. Their sensitivity is generally limited to some nT $Hz^{-1/2}$ by intrinsic electronic noise in the semiconductor [55].

Much research effort is directed toward the development of NV-center based magnetometers. They achieve sensitivities as good as 4 nT·$Hz^{-1/2}$ at room temperature [52], and magnetic field imaging [51], and magnetic resonance imaging [56] at the nanoscale. However, NV center based magnetometers have some constraints, including sensitivity to magnetic field misalignment [57], complexity of the magnetic field readout [58], and the requirement of bulky optics.

SERF magnetometers measure magnetic fields by monitoring a high density vapor of alkali metal atoms precessing in a near-zero magnetic field [59]. SERFs have been used successfully in various applications including medicine and geology, but suffer from two drawbacks. Firstly, they are relatively large with dimensions at least in the mm-range even when using micro-fabricated gas cells [45]. Secondly, they have a low dynamic range, and even at geomagnetic field strengths (≈50 μT) are adversely affected by the non-linear Zeeman effect [11, 16].

In SQUIDs [11], the magnetic field induces a current in a superconducting loop containing Josephson junctions. Although they achieve excellent sensitivities, SQUIDs require cryogenic cooling, which increases operational costs, complicates applications and increases the crucial distance between sensor and sample.

Magnetostrictive magnetometers provide a possible avenue towards miniaturization and integration of room temperature magnetometers. Magnetic fields induce mechanical stress in the sensor material. This stress is measured either electrically using a piezoelectric mechanism or optically using interferometry. Unlike other classes of magnetic field sensors, magnetostrictive magnetometers exist in a broad range of sizes, ranging from microscopic Terfenol-D coated micro-cantilevers to fiber interferometers with sensitivities of fT·$Hz^{-1/2}$ and sizes of several centimeters, which shows their extraordinary flexibility. The design presented in [19, 20] had two major advantages when compared to other magnetostrictive based magnetic field sensors. Firstly, the optical field, which is used for measurement, is strongly amplified locally by using an optical cavity. Secondly, the mechanical strain,

which originates from the magnetostrictive mechanism, is enhanced by the mechanical eigenmodes of the system. An optomechanical magnetometer could potentially outperform conventional magnetometers in its volume range, including cryogenic SQUIDs.

5. Conclusions

We have presented a technique to predict the sensitivity of cavity optomechanical field sensors. This technique could be used to optimize the design of these sensors. Furthermore, we have shown that the sensitivity of magnetostrictive magnetometers can be greatly enhanced by introducing an optomechanical cavity to detect the induced magnetostrictive stress. Such a magnetostrictive based cavity optomechanical magnetometer can potentially outperform state-of-the-art sensors of comparable size.

Acknowledgment

The authors acknowledge valuable advice from Stefan Prams, Erik van Ooijen, Glen Harris, George Brawley, Michael Taylor and Alex Szorkovszky; and financial support from the Australian Research Council through Discovery Project DP0987146.

References

[1] A. Edelstein, "Advances in magnetometry," *Journal of Physics: Condensed Matter*, vol. 19, no. 16, pp. 165217, 2007.

[2] M. Diaz-Michelena, "Small magnetic sensors for space applications," *Sensors*, vol. 9, no. 4, pp. 2271–2288, 2009.

[3] P. Ripka and M. Janosek, "Advances in magnetic field sensors," *IEEE Sensors Journal*, vol. 10, no. 6, pp. 1108–1116, 2010.

[4] F. Bucholtz, D. M. Dagenais, and K. P. Koo, "High-frequency fibre-optic magnetometer with $70\,\mathrm{fT}/\sqrt{(Hz)}$ resolution," *Electronics Letters*, vol. 25, no. 25, pp. 1719–1721, 1989.

[5] H. J. Mamin, M. Poggio, C. L. Degen, and D. Rugar, "Nuclear magnetic resonance imaging with 90-nm resolution," *Nature Nanotechnology*, vol. 2, no. 5, pp. 301–306, 2007.

[6] V. Pizzella, S. D. Penna, C. D. Gratta, and G. L. Romani, "SQUID systems for biomagnetic imaging," *Superconductor Science and Technology*, vol. 14, no. 7, pp. R79–R114, 2001.

[7] A. M. Chang, H. D. Hallen, L. Harriott, H. F. Hess, H. L. Kao, J. Kwo, *et al*., "Scanning Hall probe microscopy," *Applied Physics Letters*, vol. 61, no. 16, pp. 1974–1976, 1992.

[8] H. B. Dang, A. C. Maloof, and M. V. Romalis, "Ultrahigh sensitivity magnetic field and magnetization measurements with an atomic magnetometer," *Applied Physics Letters*, vol. 97, no. 15, pp. 151110-1–151110-3, 2010.

[9] J. M. Taylor, P. Cappellaro, L. Childress, L. Jiang, D. Budker, P. R. Hemmer, *et al*., "High-sensitivity diamond magnetometer with nanoscale resolution," *Nature Physics*, vol. 4, no. 10, pp. 810–816, 2008.

[10] M. Vengalattore, J. M. Higbie, S. R. Leslie, J. Guzman, L. E. Sadler, and D. M. Stamper-Kurn, "High-resolution magnetometry with a spinor Bose-Einstein condensate," *Physical Review Letters*, vol. 98, no. 20, pp. 200801, 2007.

[11] M. V. Romalis and H. B. Dang, "Atomic magnetometers for materials characterization," *Materials Today*, vol. 14, no. 6, pp. 258–262, 2011.

[12] S. Xu, V. V. Yashchuk, M. H. Donaldson, S. M. Rochester, D. Budker, and A. Pines, "Magnetic resonance imaging with an optical atomic magnetometer," in *Proceedings of the National Academy of Sciences*, vol. 103, no. 34, pp. 12668–12671, 2006.

[13] M. P. Ledbetter, T. Theis, J. W. Blanchard, H. Ring, P. Ganssle, S. Appelt, *et al*., "Near-zero-field nuclear magnetic resonance," *Physical Review Letters*, vol. 107, no. 10, pp. 107601, 2011.

[14] J. Jang, R. Budakian, and Y. Maeno, "Phase-locked cantilever magnetometry," *Applied Physics Letters*, vol. 98, no. 13, pp. 132510, 2011.

[15] L. S. Bouchard, V. M. Acosta, E. Bauch, and D. Budker, "Detection of the Meissner effect with a diamond magnetometer," *New Journal of Physics*, vol. 13, pp. 025017, 2011.

[16] D. Budker and M. Romalis, "Optical magnetometry," *Nature Physics*, vol. 3, no. 4, pp. 227–234, 2007.

[17] M. Hämäläinen, R. Hari, R. J. Ilmoniemi, J. Knuutila, and O. V. Lounasmaa, "Magnetoencephalography – theory, instrumentation,

and applications to noninvasive studies of the working human brain," *Reviews of Modern Physics*, vol. 65, no. 2, pp. 413–497, 1993.

[18] S. Palva and J. M. Palva, "New vistas for alpha-frequency band oscillations," *Trends in Neurosciences*, vol. 30, no. 4, pp. 150–158, 2007.

[19] S. Forstner, S. Prams, J. Knittel, E. D. van Ooijen, J. D. Swaim, G. I. Harris, *et al*., "Cavity optomechanical magnetometer," *Physics Review Letters*, vol. 108, no. 12, pp. 120801, 2012.

[20] S. Forstner, J. Knittel, H. Rubinsztein-Dunlop, and W. P. Bowen, "Model of a microtoroidal magnetometer," in *Proc. SPIE*, vol. 8439, pp. 84390U, 2012.

[21] J. Knittel, S. Forstner, J. Swaim, H. Rubinsztein-Dunlop, and W. P. Bowen, "Sensitivity of cavity optomechanical field sensors," in *Proc. SPIE*, vol. 8351, pp. 83510H, 2012.

[22] T. Corbitt and N. Mavalvala, "Quantum noise in gravitational-wave interferometers," *Journal of Optics B: Quantum and Semiclassical Optics*, vol. 6, no. 8, pp. S675–S683, 2004.

[23] V. B. Braginsky, *Measurement of weak forces in physics experiments*. Chicago: University of Chicago Press. 1977.

[24] T. J. Kippenberg and K. J. Vahala, "Cavity opto-mechanics," *Optics Express*, vol. 15, no. 25, pp. 17172–17205, 2007.

[25] T. J. Kippenberg and K. J. Vahala, "Cavity optomechanics: back-action at the mesoscale," *Science*, vol. 321, no. 5893, pp. 1172–1176, 2008.

[26] J. D. Teufel, T. Donner, D. Li, J. W. Harlow, M. S. Allman, K. Cicak, *et al*., "Sideband cooling of micromechanical motion to the quantum ground state," *Nature*, vol. 475, no. 7356, pp. 359–363, 2011.

[27] J. Chan, T. P. M. Alegre, A. H. Safavi-Naeini, J. T. Hill, A. Krause, S. Groeblacher, *et al*., "Laser cooling of a nanomechanical oscillator into its quantum ground state," *Nature*, vol. 478, no. 7367, pp. 89–92, 2011.

[28] A. Schliesser, G. Anetsberger, R. Riviere, O. Arcizet, and T. J. Kippenberg, "High-sensitivity monitoring of micromechanical vibration using optical whispering gallery mode resonators," *New Journal of Physics*, vol. 10, no. 9, pp. 095015, 2008.

[29] C. A. Regal, J. D. Teufel, and K. W. Lehnert, "Measuring nanomechanical motion with a microwave cavity interferometer," *Nature Physics*, vol. 4, no. 7, pp. 555–560, 2008.

[30] A. H. Safavi-Naeini, J. Chan, J. T. Hill, T. P. M. Alegre, A. Krause, and O. Painter, "Observation of quantum motion of a nanomechanical resonator," *Physical Review Letters* vol. 108, no. 3, pp. 033602, 2012.

[31] J. Liu, K. Usami, A. Naesby, T. Bagci, E. S. Polzik, P. Lodahl, *et al*., "High-*Q* optomechanical GaAs nanomembranes," *Applied Physics Letters,* vol. 99, no. 24, pp. 243102, 2011.

[32] H. Cai and A. W. Poon, "Optical manipulation of microparticles using whispering-gallery modes in a silicon nitride microdisk resonator," *Optics Letters*, vol. 36, no. 21, pp. 4257–4259, 2011.

[33] C. P. Dietrich, M. Lange, C. Sturm, R. Schmidt-Grund, and M. Grundmann,"One- and two-dimensional cavity modes in ZnO microwires," *New Journal of Physics*, vol. 13, no. 10, pp. 103021–103029, 2011.

[34] D. Kleckner, B. Pepper, E. Jeffrey, P. Sonin, S. M. Thon, and D. Bouwmeester, "Optomechanical trampoline resonators," *Optics Express*, vol. 19, no. 20, pp. 19708–19716, 2011.

[35] A. G. Kuhn, M. Bahriz, O. Ducloux, C. Chartier, O. L. Traon, T. Briant, *et al*., "A micropillar for cavity optomechanics," *Applied Physics Letters*, vol. 99, no. 12, pp. 121103, 2011.

[36] I. Wilson-Rae, C. Galland, W. Zwerger, and A. Imamoglu, "Nano-optomechanics with localized carbon-nanotube excitons," *arXiv: 0911.1330v1 [cond-mat.mes-hall]*, 2009.

[37] B. P. Abbott, R. Abbott, R. Adhikari, P. Ajith, B. Allen, G Allen, *et al*., "LIGO: the laser interferometer gravitational-wave observatory," *Reports on Progress in Physics*, vol. 72, no. 7, pp. 076901, 2009.

[38] L. D. Landau and E. M. Lifshitz, *Theory of elasticity (Course of Theoretical Physics)*, 2nd edition, vol. 7. Oxford: Pergamon Press, 1970.

[39] D. T. Gillespie, "The mathematics of Brownian motion and Johnson noise," *American Journal of Physics*, vol. 64, no. 3, pp. 225–240, 1996.

[40] A. Schliesser, "Cavity optomechanics and optical frequency comb generation with silica whispering-gallery-mode microresonators," Ph.D. dissertation, Physik. Department, Ludwig-Maximilians-Universität, 2009.

[41] V. B. Braginsky, S. E. Strigin, and V. P. Vyatchanin, "Parametric oscillatory instability in Fabry-Perot interferometer," *Physics Letters A*, vol. 287, no. 5–6, pp. 331–338, 2001.

[42] M. Pinard, Y. Hadjar, and A. Heidmann, "Effective mass in quantum effects of radiation pressure," *The European Physical Journal D–Atomic, Molecular, Optical and Plasma Physics*, vol. 7, no. 1, pp. 107–116, 1999.

[43] V. Giovannetti and D. Vitali, "Phase-noise measurement in a cavity with a movable mirror undergoing quantum Brownian motion," *Physical Review A*, vol. 63, no. 2, pp. 023812, 2001.

[44] V. B. Braginsky and F. Y. Khalili, *Quantum Measurement*. Cambridge: Cambridge University Press, 1992.

[45] D. Maser, S. Pandey, H. Ring, M. P. Ledbetter, S. Knappe, J. Kitching, *et al*., "Note: detection of a

single cobalt microparticle with a microfabricated atomic magnetometer," *Review of Scientific Instruments*, vol. 82, no. 8, pp. 086112, 2011.

[46] J. R. Kirtley, M. B. Ketchen, K. G. Stawiasz, J. Z. Sun, W. J. Gallagher, S. H. Blanton, *et al*., "High-resolution scanning squid microscope," *Applied Physics Letters*, vol. 66, no. 9, pp. 1138–1140, 1995.

[47] M. I. Faley, U. Poppe, K. Urban, D. N. Paulson, and R. L. Fagaly, "A new generation of the HTS multilayer dc-squid magnetometers and gradiometers," *Journal of Physics: Conference Series*, vol. 43, no. 1, pp. 1199–1202, 2006.

[48] F. Baudenbacher, L. E. Fong, J. R. Holzer, and M. Radparvar, "Monolithic low-transition temperature superconducting magnetometers for high resolution imaging magnetic fields of room temperature samples," *Applied Physics Letters*, vol. 82, no. 20, pp. 3487–3489, 2003.

[49] A. Sandhu, A. Okamoto, I. Shibasaki, and A. Oral, "Nano and micro Hall-effect sensors for room-temperature scanning Hall probe microscopy," *Microelectronic Engineering*, vol. 73–74, pp. 524–528, 2004.

[50] A. Sandhu, K. Kurosawa, M. Dede, and A. Oral, "50 nm Hall sensors for room temperature scanning Hall probe microscopy," *Japanese Journal of Applied Physics*, vol. 43, no. 2, pp. 777–778, 2004.

[51] J. R. Maze, P. L. Stanwix, J. S. Hodges, S. Hong, J. M. Taylor, P. Cappellaro, *et al*., "Nanoscale magnetic sensing with an individual electronic spin in diamond," *Nature*, vol. 455, no. 7213, pp. 644–647, 2008.

[52] G. Balasubramanian, P. Neumann, D. Twitchen, M. Markham, R. Kolesov, N. Mizuochi, *et al*., "Ultralong spin coherence time in isotopically engineered diamond," *Nature Materials*, vol. 8, no. 5, pp. 383–387, 2009.

[53] S. X. Dong, J. F. Li, and D. Viehland, "Ultrahigh magnetic field sensitivity in laminates of terfenol-D and $Pb(Mg_{1/3}Nb_{2/3})O_3$-$PbTiO_3$ crystals," *Applied Physics Letters*, vol. 83, no. 11, pp. 2265–2267, 2003.

[54] R. Osiander, S. A. Ecelberger, R. B. Givens, D. K. Wickenden, J. C. Murphy, and T. J. Kistenmacher, "A microelectromechanical-based magnetostrictive magnetometer," *Applied Physics Letters*, vol. 69, no. 19, pp. 2930–2931, 1996.

[55] K. Vervaeke, E. Simoen, G. Borghs, and V. V. Moshchalkov, "Size dependence of microscopic Hall sensor detection limits," *Review of Scientific Instruments*, vol. 80, no. 7, pp. 074701-1–074701-7, 2009.

[56] M. S. Grinolds, P. Maletinsky, S. Hong, M. D. Lukin, R. L. Walsworth, and A. Yacoby, "Quantum control of proximal spins using nanoscale magnetic resonance imaging," *Nature Physics*, vol. 7, no. 9, pp. 687–692, 2011.

[57] L. M. Pham, D. L. Sage, P. L. Stanwix, T. K. Yeung, D. Glenn, A. Trifonov, *et al*., "Magnetic field imaging with nitrogen-vacancy ensembles," *New Journal of Physics*, vol. 13, pp. 045021, no. 4, 2011.

[58] R. S. Schoenfeld and W. Harneit, "Real time magnetic field sensing and imaging using a single spin in diamond," *Physical Review Letters*, vol. 106, no. 3, pp. 030802, 2011.

[59] J. C. Allred, R. N. Lyman, W. Kornack, and M. V. Romalis, "High-sensitivity atomic magnetometer unaffected by spin-exchange relaxation," *Physical Review Letters*, vol. 89, no. 13, pp. 130801, 2002.